Mathematical modelling, bifurcation analysis, circuit design and FPGA implementation of a 5-D hyperchaotic weather fluctuation model with a line of equilibrium points

Sundarapandian Vaidyanathan*

Centre for Control Systems, Vel Tech University
400 Feet Outer Ring Road, Avadi, Chennai-600062
Tamil Nadu, India
E-mail: sundarcontrol@gmail.com
*Corresponding author

Irene M. Moroz

Mathematical Institute, University of Oxford
Oxford OX2 6GG, England, UK.
E-mail: Irene.Moroz@maths.ox.ac.uk

Esteban Tlelo-Cuautle

Department of Electronics
The National Institute of Astrophysics, Optics and Electronics (INAOE)
Tonantzintla, Puebla 72840, Mexico.
E-mail: etlelo@inaoep.mx

Aceng Sambas

Department of Mechanical Engineering
Universitas Muhammadiyah Tasikmalaya
Tasikmalaya 46196, West Java
Indonesia
E-mail: acengs@umtas.ac.id

Ciro Fabian Bermudez-Marquez

Department of Electronics
The National Institute of Astrophysics, Optics and Electronics (INAOE)
Tonantzintla, Puebla 72840, Mexico.
E-mail: cirofabian.bermudez@gmail.com

Samy Abdelwahab Safaan

Department of Natural and Applied Sciences
Community College of Buraydah, Qassim University
Buraydah, 52571, Saudi Arabia
and
Nile Higher Institute for Commercial Science and Computer Technology
Mansoura, 35511, Egypt
E-mail: safan@qu.edu.sa

Abstract: High-dimensional hyperchaotic systems are known to have several applications in engineering owing to their high complexity. This work reports the finding of a new 5-D hyperchaotic weather fluctuation model, which is constructed by means of introducing two state feedback controllers in the 3-D Vallis weather fluctuation model (1986). The new hyperchaotic system has a line of equilibrium points. Hence, it has hidden attractors. We carry out a detailed bifurcation analysis with standard tools such as bifurcation diagrams and Lyapunov exponents to study the intrinsic properties of the 5-D weather fluctuation model with respect to changes in the system constants. Next, we design an electronic circuit of the 5-D weather fluctuation model using MultiSim. The new 5-D hyperchaotic weather fluctuation model is implemented herein by applying two one-step numerical methods, *viz.* Forward Euler and Trapezoidal rule. Experimental attractors for the 5-D hyperchaotic model are shown from an oscilloscope.

1 Introduction

Scientific modelling and engineering applications of dynamical systems are miscellaneous topics of research (Thomas and Mija, 2022; Tang and Liu, 2022; Okasha et al., 2022; Dachraoui et al., 2022; Qian et al., 2022; Wu et al., 2022; Gaouzi et al., 2022; Hassani et al., 2022; Zahorán and Kovács, 2022; Tiglio and Villanueva, 2022; Ratier and Charles, 2022; Bae and Koumoutsakos, 2022; Lopez-Rodriguez and Ceballos, 2022; Meng and Shao, 2022). Computer simulation of dynamical systems aids the modelling, design and implementation of associated control systems (Almasoud, 2023; Yoon and Kim, 2022; Tanaka and Nakane, 2022; Fujita and Tanaka, 2022). With the rapid advances of chaos theory, the modelling, and engineering applications o hyperchaotic systems are important topics in research (Cai and He, 2022; Bhat and Moon, 2022; Dong and Wang, 2022; Doungmo Goufo, 2022; Liu and Wang, 2022; Petrzela, 2022). Cai and He (2022) presented an image encryption algorithm and multiple pseudo-random sequences built on a controlled hyperchaotic system. Bhat and Moon (2022) dealt with a 4-D hyperchaotic system for the image encryption and authentication based on pseudo-random sequences using dynamic DNA encoding. Dong and Wang (2022) studied hidden chaotic and hyperchaotic attractors of a multistable hyperchaotic system and designed an electronic circuit for it. Doungmo Goufo (2022) analysed fractal design for multiwing hyperchaotic systems comprising a linear or rotational self-duplication process occurring in different scales across the hyperchaotic system and resulting with the triangular or square shape. Liu and Wang (2022) suggested an hyperchaotic electronic circuit with a meminductor, memcapacitor, and memristor and analysed the qualitative properties using the classical methods. Petrzela (2022) studied the Clapp hyperchaotic attractor designed using a generalized bipolar transistor as an active element.

High-dimensional hyperchaotic systems are known to have several applications in engineering fields owing to their high complexity (Cai and He, 2022; Bhat and Moon, 2022; Doungmo Goufo, 2022; Liu and Wang, 2022; Petrzela, 2022; Fu and Lei, 2022; Zhang and Huang, 2022; Peng et al., 2021). Fu and Lei (2022) proposed a set of fractional-order symmetric 5-D hyperchaotic systems using the Adomian decomposition method and build an electronic 5-D hyperchaotic circuit using MultiSim (Version 14). Zhang and Huang (2022) created a 5-D Hamiltonian hyperchaotic system with four centre-type balance points. Peng et al. (2021) proposed a 5-D conservative hyperchaotic system with no balance point.

Vallis (1986) derived a chaotic system modelling the El-nino weather fluctuations associated with the warm ocean water in the equatorial Pacific Ocean including the Pacific coast of South America. Vaidyanathan et al. (2018) derived a 4-D hyperchaotic weather fluctuation model with a unique balance point at the origin by means of introducing a state feedback controller to the Vallis chaotic system (Vallis, 1986). A main result of this work is the modelling of a 5-D hyperchaotic weather fluctuation model with three positive Lyapunov exponents and a line of balance points obtained by introducing a state feedback controller to the 4-D hyperchaotic weather fluctuation system (Vaidyanathan et al., 2018). We also calculated the Kaplan-Yorke dimension of the new 5-D hyperchaotic weather fluctuation model. Kaplan-Yorke dimension gives a significant insight into the information dimension for a given chaotic or hyperchaotic system (Frederickson et al., 1983; Chen, 1993; Nichols et al., 2003).

We carry out a detailed bifurcation analysis with standard tools such as bifurcation diagrams and Lyapunov exponents to study the intrinsic properties of the 5-D weather fluctuation model with respect to changes in the system constants. Next, we design an electronic circuit of the 5-D weather fluctuation model using MultiSim (Version 14). It is well-known that circuit design of hyperchaotic attractors aids the implementation of such systems in engineering applications (Petrzela, 2022; Petrzela and Rujzl, 2022; Fu and Lei, 2022; Bhardwaj and Srivastava, 2022; Vaidyanathan et al., 2018).

The new hyperchaotic weather fluctuation model can be implemented with different electronic hardware such as field-programmable analog array (FPAA) (Silva-Juarez et al., 2022), field-programmable gate array (FPGA) (Vaidyanathan et al., 2021), discrete amplifiers, and even using integrated circuit technology, as shown in (Carbajal-Gomez et al., 2019). Implementations based on discrete amplifiers can be improved using FPAAs, however, both cases can reach very low frequencies compared to using FPGAs. In this manner, this work shows the FPGA implementation applying two numerical methods, as detailed in Section 5.

2 A 5-D hyperchaotic weather fluctuation model

Vallis (1986) reported a 3-D dynamical system that models the El-nino weather fluctuations associated with the warm ocean water in the equatorial Pacific Ocean including the Pacific coast of South America.

$$\begin{cases} \dot{y}_1 = -ay_1 + by_2 \\ \dot{y}_2 = y_1 - y_2 + y_1 y_3 \\ \dot{y}_3 = -y_3 - y_1 y_2 \end{cases} \tag{1}$$

Vallis (Vallis, 1986) established that the system (1) has a chaotic attractor when $(a, b) = (5, 122)$.

For $Y(0) = (0.1, 0.4, 0.2)$, the Lyapunov exponents (LE) of the Vallis system (1) were calculated for $T = 1E5s$ as follows:

$$\begin{cases} \mu_1 = 0.5232, \\ \mu_2 = 0, \\ \mu_3 = -7.5232 \end{cases} \tag{2}$$

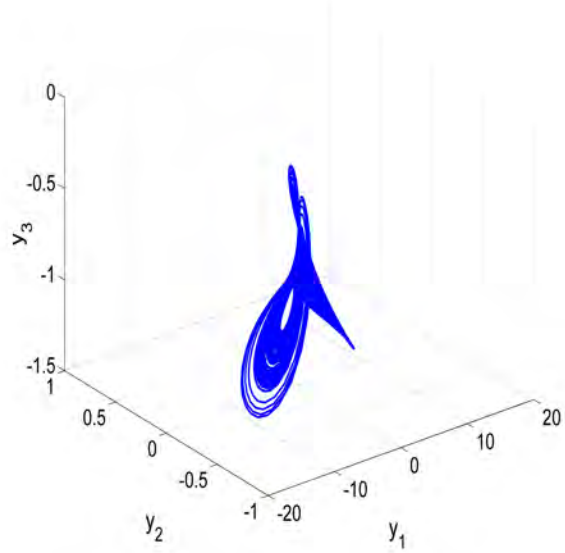

Figure 1: Signal plot simulated in Matlab for the 3-D Vallis weather fluctuation chaotic system (1) for $(a, b) = (5, 122)$ and $Y(0) = (0.1, 0.4, 0.2)$

Figure 1 deploys the two-scroll chaotic attractor of the 3-D Vallis weather fluctuation chaotic system (1).

Vaidyanathan et al. (2018) derived a 4-D hyperchaotic weather fluctuation system by means of introducing a state feedback controller in the Vallis system (1), which can be stated as follows:

$$\begin{cases} \dot{y}_1 = -ay_1 + by_2 + y_4 \\ \dot{y}_2 = y_1 - y_2 + y_1 y_3 \\ \dot{y}_3 = -y_3 - y_1 y_2 \\ \dot{y}_4 = -cy_1 \end{cases} \tag{3}$$

Vaidyanathan et al. (2018) observed that the 4-D weather fluctuation system model (3) has a hyperchaotic attractor when $(a, b, c) = (10, 150, 2)$.

For $Y(0) = (0.1, 0.4, 0.2, 0.3)$, the LE values of the 4-D Vaidyanathan weather fluctuation system (3) were calculated for $T = 1E5s$ as follows:

$$\begin{cases} \mu_1 = 0.1232, \\ \mu_2 = 0.1008, \\ \mu_3 = 0, \\ \mu_4 = -12.2957. \end{cases} \tag{4}$$

It can be easily checked that $Y_0 = (0, 0, 0, 0)$ is the unique balance point of the 4-D Vaidyanathan hyperchaotic weather fluctuation system (3).

Figures 2 and 3 deploy the two-scroll hyperchaotic attractor of the 4-D Vaidyanathan hyperchaotic weather fluctuation system (3) in (y_1, y_2, y_3) space and (y_2, y_3, y_4) space respectively.

We propose a new 5-D weather fluctuation model in this work by means of introducing two state feedback

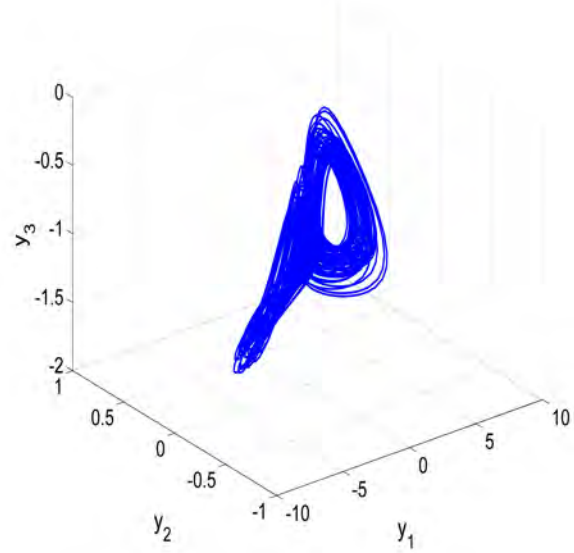

Figure 2: Signal plot simulated in Matlab for the 4-D Vaidyanathan hyperchaotic weather fluctuation system (3) for $(a, b, c) = (10, 150, 2)$ and $Y(0) = (0.1, 0.4, 0.2, 0.3)$ in (y_1, y_2, y_3) space

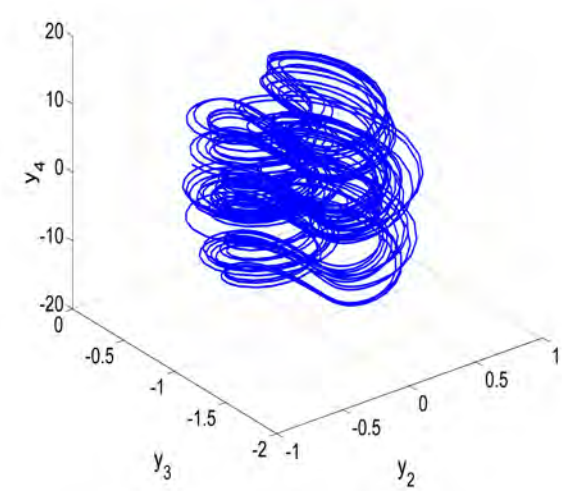

Figure 3: Signal plot simulated in Matlab for 4-D Vaidyanathan hyperchaotic weather fluctuation system (3) for $(a, b, c) = (10, 150, 2)$and $Y(0) = (0.1, 0.4, 0.2, 0.3)$ in (y_2, y_3, y_4) space

controllers in the 3-D Vallis weather fluctuation model (1), which is stated as follows:

$$\begin{cases} \dot{y}_1 = -ay_1 + by_2 + y_4 + py_5 \\ \dot{y}_2 = y_1 - y_2 + y_1 y_3 \\ \dot{y}_3 = -y_3 - y_1 y_2 \\ \dot{y}_4 = -c(y_1 + y_2) \\ \dot{y}_5 = -dy_2 \end{cases} \tag{5}$$

We denote the state of the 5-D system (5) as follows:

$$Y = (y_1, y_2, y_3, y_4, y_5) \tag{6}$$

In the model (5), a, b, c, d, p are assumed to be positive constants.

We shall show that the 5-D system (5) has a hyperchaotic attractor with three positive LE values for the parameter values

$$a = 5, b = 125, c = 0.5, d = 2, p = 2.5 \tag{7}$$

For $Y(0) = (0.1, 0.4, 0.2, 0.3, 0.1)$, the LE values of the 5-D weather fluctuation system (5) were calculated for $T = 1E5s$ as follows:

$$\begin{cases} \mu_1 = 0.5046, \\ \mu_2 = 0.0134, \\ \mu_3 = 0.0114, \\ \mu_4 = 0, \\ \mu_5 = -7.5253 \end{cases} \tag{8}$$

This calculation using MATLAB establishes that the 5-D weather fluctuation system (5) is hyperchaotic with 3 positive LE values.

We observe that the Vallis system (1) has only two quadratic nonlinearities, *viz.* y_1y_2 and y_1y_3. Morever, the new 5-D hyperchaotic weather fluctuation model (5) also has two quadratic nonlinearities, *viz.* y_1y_2 and y_1y_3. Thus, retaining the same nonlinearities as the Vallis system (Vallis, 1986), we have derived a new 5-D hyperchaotic system with more complexities, *viz.* 3 positive LE values.

Next, we calculate the Kaplan-Yorke dimension of the 5-D hyperchaotic weather fluctuation system (5) as given below:

$$D_{KY} = 4 + \frac{\mu_1 + \mu_2 + \mu_3 + \mu_4}{|\mu_5|} = 4.0703 \tag{9}$$

The high value of D_{KY} for the 5-D system (5) pinpoints the high complexity of the system, which makes it very suitable for secure communication applications involving complex dynamical systems.

The balance points of the 5-D system (5) are found by solving the following system of algebraic equations.

$$-ay_1 + by_2 + y_4 + py_5 = 0 \tag{10a}$$

$$y_1 - y_2 + y_1y_3 = 0 \tag{10b}$$

$$-y_3 - y_1y_2 = 0 \tag{10c}$$

$$-c(y_1 + y_2) = 0 \tag{10d}$$

$$-dy_2 = 0 \tag{10e}$$

From (10e), $y_2 = 0$.

Substituting $y_2 = 0$ into (10d), we get $y_1 = 0$.

Substituting $y_1 = y_2 = 0$ into (10c), we get $y_3 = 0$.

Substituting $y_1 = y_2 = y_3 = 0$ into (10a), we get

$$y_4 + py_5 = 0 \tag{11}$$

We note that $p > 0$.

Thus, we conclude that the 5-D system (5) has a line of equilibrium points, which is defined by

$$S = \{y \in \mathbf{R}^5 : y_1 = y_2 = y_3 = 0, y_4 + py_5 = 0\} \tag{12}$$

In the hyperchaotic case (7), $p = 2.5$.

Figure 4 shows the line equilibrium ($y_4 + py_5 = 0$) of the 5-D hyperchaotic system (5) in the (y_4, y_5) plane when $p = 2.5$.

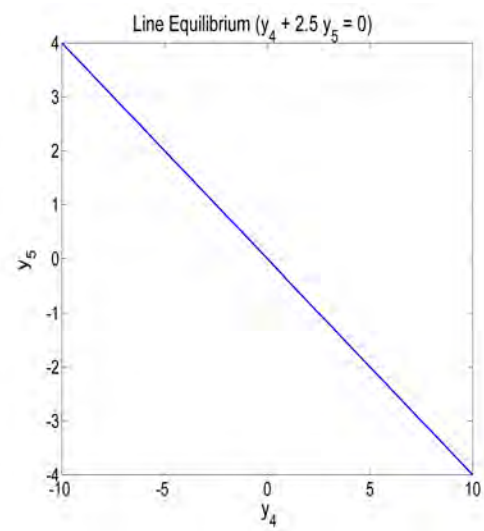

Figure 4: Line equilibrium ($y_4 + py_5 = 0$) of the 5-D hyperchaotic weather fluctuation model (5) in the (y_4, y_5) plane when $p = 2.5$.

Hence, the 5-D hyperchaotic temperature fluctuation system (5) has hidden attractors.

Figures 5, 6, 7 and 8 deploy the two-scroll hyperchaotic attractor of the 5-D hyperchaotic weather fluctuation system (5) in (y_1, y_2)-plane, (y_1, y_3)-plane, (y_1, y_4)-plane and (y_1, y_5)-plane, respectively.

Multistability of a hyperchaotic system refers to the coexistence of two or more hyperchaotic attractors for the same set of values for the system parameters but different values of the initial states of the system. Interestingly, the new 5-D hyperchaotic weather fluctuation system (5) exhibits multistability, which can be seen by considering the same set of values $(a, b, c, d, p) = (5, 125, 0.5, 2, 2.5)$ for the 5-D hyperchaotic weather fluctuation system (5) but two different initial states $Y_0 = (0.1, 0.4, 0.2, 0.3, 0.1)$ and $Z_0 = (-0.2, 0.4, 0.2, 0.3, -0.2)$. Figures 9 and 10 show the multistability of the 5-D hyperchaotic weather fluctuation system (5) in (y_1, y_2) plane and (y_3, y_5) plane respectively, where the blue orbit starts from the initial state Y_0 and the red orbit starts from the initial state Z_0.

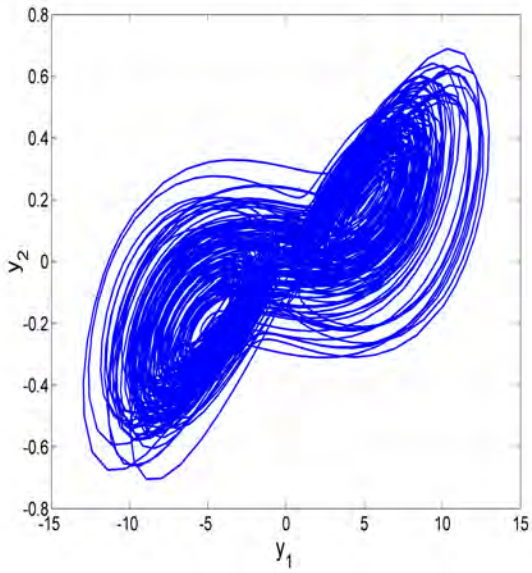

Figure 5: Signal plot simulated in Matlab for the 5-D hyperchaotic weather fluctuation system (5) for $(a, b, c, d, p) = (5, 125, 0.5, 2, 2.5)$ and $Y(0) = (0.1, 0.4, 0.2, 0.3, 0.1)$ in (y_1, y_2) plane

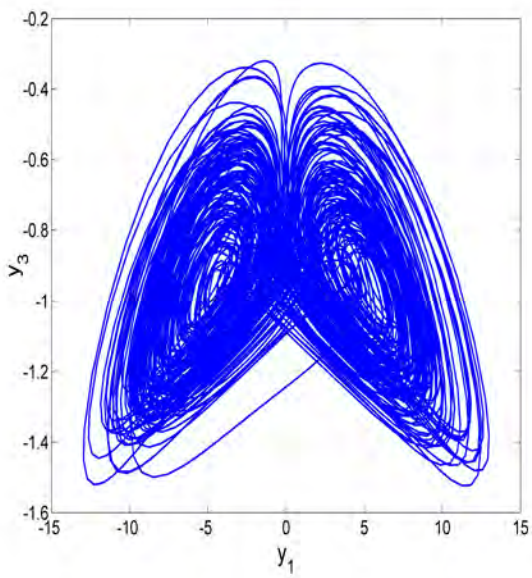

Figure 6: Signal plot simulated in Matlab for the 5-D hyperchaotic weather fluctuation system (5) for $(a, b, c, d, p) = (5, 125, 0.5, 2, 2.5)$ and $Y(0) = (0.1, 0.4, 0.2, 0.3, 0.1)$ in (y_1, y_3) plane

3 Bifurcation analysis of the 5-D hyperchaotic weather fluctuation model

3.1 The two hyperchaotic temperature fluctuation systems

The new five-dimensional system (5) takes the form:

$$\dot{y}_1 = -ay_1 + by_2 + y_4 + py_5 = F(y_1, y_2, y_3, y_4, y_5) \quad (13a)$$

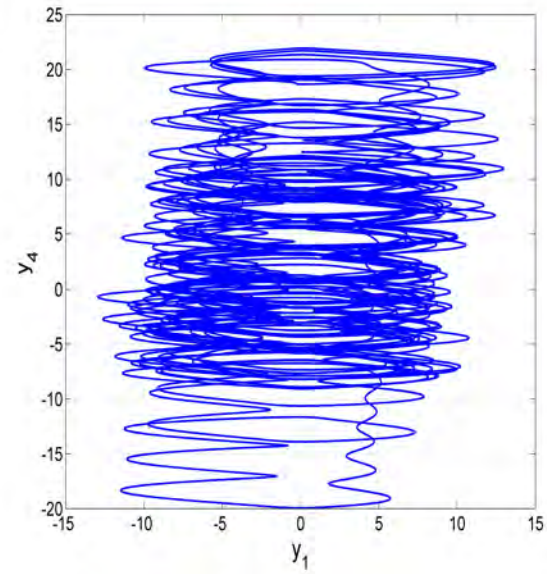

Figure 7: Signal plot simulated in Matlab for the 5-D hyperchaotic weather fluctuation system (5) for $(a, b, c, d, p) = (5, 125, 0.5, 2, 2.5)$ and $Y(0) = (0.1, 0.4, 0.2, 0.3, 0.1)$ in (y_1, y_4) plane

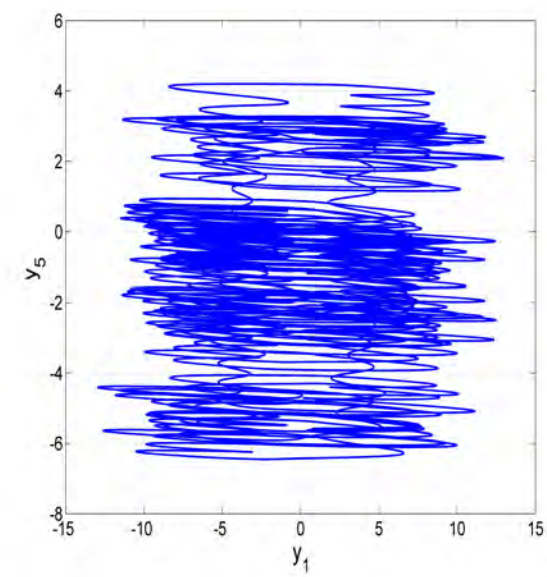

Figure 8: Signal plot simulated in Matlab for the 5-D hyperchaotic weather fluctuation system (5) for $(a, b, c, d, p) = (5, 125, 0.5, 2, 2.5)$ and $Y(0) = (0.1, 0.4, 0.2, 0.3, 0.1)$ in (y_1, y_5) plane

$$\dot{y}_2 = y_1 - y_2 + y_1 y_3 = G(y_1, y_2, y_3, y_4, y_5) \quad (13b)$$

$$\dot{y}_3 = -y_3 - y_1 y_2 = H(y_1, y_2, y_3, y_4, y_5) \quad (13c)$$

$$\dot{y}_4 = -c(y_1 + y_2) = K(y_1, y_2, y_3, y_4, y_5) \quad (13d)$$

$$\dot{y}_5 = -dy_2 = L(y_1, y_2, y_3, y_4, y_5) \quad (13e)$$

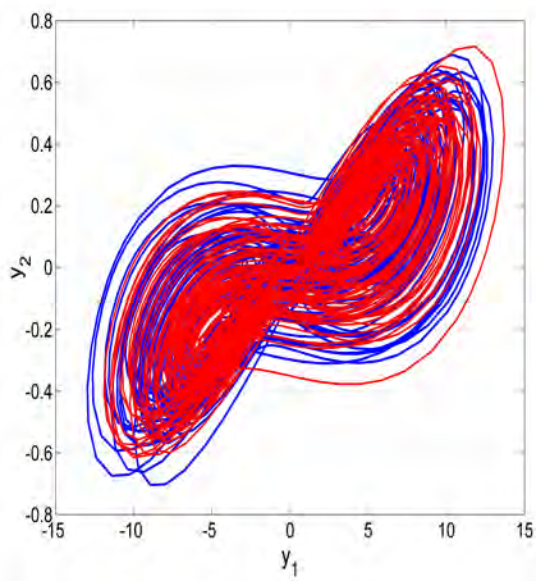

Figure 9: Multistability of the 5-D hyperchaotic weather fluctuation system (5) in the (y_1, y_2) plane for $(a, b, c, d, p) = (5, 125, 0.5, 2, 2.5)$, Initial State $Y_0 = (0.1, 0.4, 0.2, 0.3, 0.1)$ (blue orbit) and Initial State $Z_0 = (-0.2, 0.4, 0.2, 0.3, -0.2)$ (red orbit).

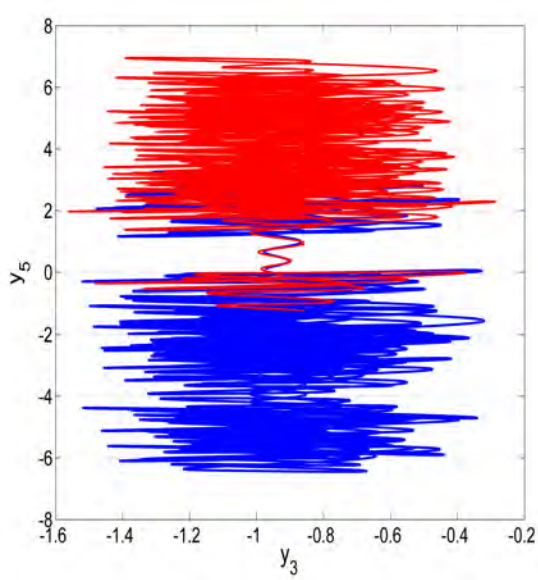

Figure 10: Multistability of the 5-D hyperchaotic weather fluctuation system (5) in the (y_3, y_5) plane for $(a, b, c, d, p) = (5, 125, 0.5, 2, 2.5)$, Initial State $Y_0 = (0.1, 0.4, 0.2, 0.3, 0.1)$ (blue orbit) and Initial State $Z_0 = (-0.2, 0.4, 0.2, 0.3, -0.2)$ (red orbit).

The system (13) extends the 4-D hyperchaotic temperature fluctuation system (Vaidyanathan et al., 2018) stated as follows:

$$\dot{y}_1 = -ay_1 + by_2 + y_4 = f(y_1, y_2, y_3, y_4) \tag{14a}$$

$$\dot{y}_2 = y_1 - y_2 + y_1 y_3 = g(y_1, y_2, y_3, y_4) \tag{14b}$$

$$\dot{y}_3 = -y_3 - y_1 y_2 = h(y_1, y_2, y_3, y_4) \tag{14c}$$

$$\dot{y}_4 = -cy_1 = k(y_1, y_2, y_3, y_4) \tag{14d}$$

All of the parameter values a, b, c, d, p are taken to be positive. In what follows we will focus primarily on the five-D system (13), but draw comparisons at each stage with aspects of the four-D model (14) (Vaidyanathan et al., 2018).

The divergence of the five-D flow (13) is:

$$\frac{\partial F}{\partial y_1} + \frac{\partial G}{\partial y_2} + \frac{\partial H}{\partial y_3} + \frac{\partial K}{\partial y_4} + \frac{\partial L}{\partial y_5} = -(2 + a) \tag{15}$$

The divergence of the four-D flow (14) is:

$$\frac{\partial f}{\partial y_1} + \frac{\partial g}{\partial y_2} + \frac{\partial h}{\partial y_3} + \frac{\partial k}{\partial y_4} = -(2 + a) \tag{16}$$

Thus, we require $2 + a > 0$ for contracting flows and $2 + a = 0$ for conservative flows. For the chosen set of parameter values $(a, b, c, d, p) = (5, 125, 0.5, 2, 2.5)$, the divergence of the flow equals -7 and hence the volumes contract in the phase space. In other words, the systems (13) and (14) are both dissipative.

3.2 Linear Stability Analysis

The equilibrium points of the 5-D system (13) are found by setting the RHS of (13) to zero. This gives a line of equilibrium points

$$y_1 = 0, y_2 = 0, y_3 = 0, y_4 + py_5 = 0 \tag{17}$$

The linear stability of the equilibrium points of the 5-D system (13) are determined by computing the Jacobian matrix evaluated at the equilibrium point:

$$J = \begin{bmatrix} -a & b & 0 & 1 & p \\ 1 & -1 & 0 & 0 & 0 \\ 0 & 0 & -1 & 0 & 0 \\ -c & -c & 0 & 0 & 0 \\ 0 & -d & 0 & 0 & 0 \end{bmatrix} \tag{18}$$

and determining the roots of the characteristic equation:

$$\lambda(\lambda + 1)\varphi(\lambda) = 0 \tag{19}$$

where

$$\varphi(\lambda) = \lambda^3 + (a + 1)\lambda^2 + (a - b + c)\lambda + 2c + dp \tag{20}$$

Two eigenvalues are therefore $\lambda = 0$ and $\lambda = -1$. The remaining three eigenvalues are obtained by solving the following cubic equation $\varphi(\lambda) = 0$.

3.3 Linear stability analysis for the 5-D system

We consider the cubic equation

$$\lambda^3 + (a + 1)\lambda^2 + (a + c - b)\lambda + 2c + dp = 0 \tag{21}$$

The equation (21) will have $\lambda = 0$ as a root when $2c + dp = 0$.

However, since all parameters are assumed to be positive, $2c + dp$ is non-zero.

Hence, $\lambda = 0$ is not a root of the equation (21).

For a Hopf bifurcation, $\lambda = \pm i\omega$. Thus, we require

$$\omega^2 = \frac{2c + dp}{1 + a} = a + c - b > 0, \tag{22}$$

so that $a + c - b > 0$.

Combining these two equalities, we obtain the Hopf bifurcation curve

$$b_{HB} = \frac{a^2 + a(1 + c) - (dp + c)}{(1 + a)}, \tag{23}$$

in terms of b, or

$$a_{HB} = \frac{b-(1+c)}{2} + \frac{\sqrt{[(b-(1+c))^2+4(dp+b+c)]}}{2} \tag{24}$$

in terms of a. Note that for positive parameter choices, the value of the discriminant in Eq. (24) is greater than $b - (1 + c)$, so only the positive root applies.

One thing to note is that for the chosen set of parameter values, a Hopf bifurcation is ruled out. In order to satisfy the second relation in Eq. (22), we need to select much smaller values of b. This is also true for the reduced 4-D system.

We therefore chose $b = 12$ for this aspect of the analysis. With $c = 0.5$, we obtain $a = 11.9628$ for the Hopf bifurcation in the 5-D system, with the corresponding frequency of $\omega = 0.6803i$, with the remaining eigenvalue as $\lambda = -12.9628$.

3.4 Linear stability analysis for the 4-D system

Since Vaidyanathan et al. (2018) did not investigate the possibility of Hopf bifurcations in the 4-D model (14), we do so here.

The corresponding eigenspectrum is $\lambda = -a$, together with the cubic equation

$$\lambda^3 + (1 + a)\lambda^2 + (a - b + c)\lambda + c = 0. \tag{25}$$

Again $\lambda \neq 0$, but a Hopf bifurcation is possible when

$$\omega^2 = \frac{c}{1 + a} = a + c - b > 0, \tag{26}$$

with

$$b_{4HB} = \frac{a^2 + a(1 + c)}{(1 + a)}. \tag{27}$$

Again choosing $b = 12$, we obtain $a = 11.5399$ as the Hopf bifurcation value for the 4-D system, with frequency $\omega = \pm 0.1997i$ and $\lambda = -12.5399$.

Numerical integrations, reported in the following subsection, verify our linear stability results.

3.5 Nonlinear dynamics for the 5-D system

To explore the nonlinear dynamics, we rewrite the system (13) as follows:

$$\begin{cases} \dot{x} = -ax + by + v + pw \\ \dot{y} = x - y + xz \\ \dot{z} = -z - xy \\ \dot{v} = -c(x + y) \\ \dot{w} = -dy \end{cases} \tag{28}$$

We construct bifurcation transition diagrams as each main parameter varies in turn, as a function of x_{max}, keeping the remaining parameters at their prescribed values. Figure 11 shows the bifurcation transition plot

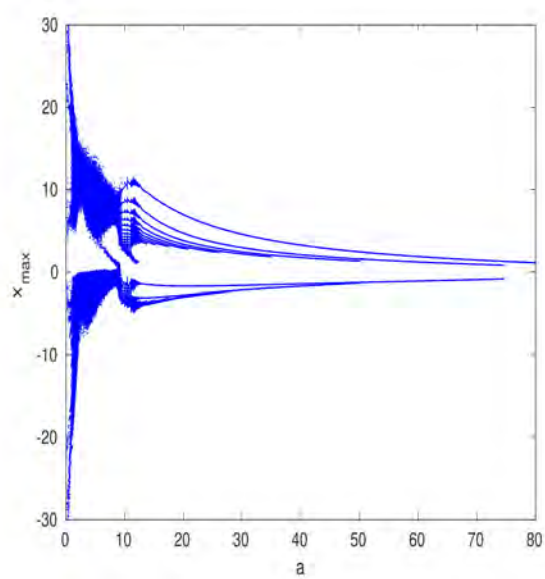

Figure 11: Part of the bifurcation transition plot of x_{max} as a decreases and increases for $b = 150$, $c = 0.5$, $d = 2$ and $p = 2.5$

of the maxima of x_{max} as a decreases from $a = 20$, with the remaining parameters given by their chosen values. We see that there is chaotic behaviour when $a = 5$, and that the amplitude of x_{max} grows without bound as $a \to 0$. There is also a transition from chaotic to multiply-periodic behaviour when $a \approx 9.5$. As a increases, the multiple branches start to disappear, leaving a single branch when $a \approx 72.25$.

Figure 12 shows the corresponding plot when b decreases from $b = 60$. The section from $b = 120$ to $b = 60$ is just chaotic. The dynamics is chaotic until $b \approx 50.25$, before the appearance of a succession of periodic windows, separated by narrow chaotic windows. With each section, two of the periodic branches disappear in period-doubling bifurcations. The first window show a period-9 branch for $44 < b < 50.25$; this gives rise to a period-7 window for $37.05 < b < 43.7$, followed by

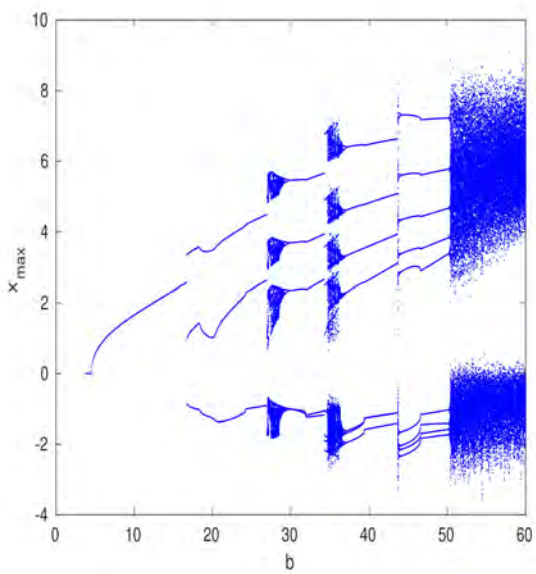

Figure 12: Bifurcation transition plot of x_{max} as b decreases.

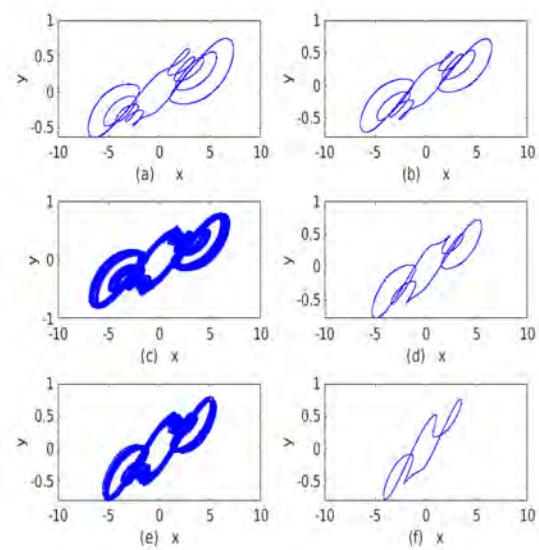

Figure 13: A selection of (x, y)-phase portraits, illustrating the dynamics in 4 periodic windows and 2 chaotic windows, shown in Figure 2 as b decreases. The plots are for: (a) $b = 45$; (b) $b = 40$; (c) $b = 35$; (d) $b = 30$; (e) $b = 28$; (f) $b = 20$.

a period-doubling and chaotic branch. Then a period-5 window appears in $29.6 < 34.55$, with its period-doubling sequence and chaotic branch, followed by a period-3 window in $16.75 < b < 26.9$. This last window terminates in a period-1 orbit until it disappears in a Hopf bifurcation at $b = 4.5$. If we substitute the values for $(a, c, d, p) = (5, 0.5, 2.0, 2.5)$ into Eq. (23), we obtain at $b_{HB} = 4.5$, thereby verifying the predictions of the linear stability bifurcation analysis.

Varying the remaining parameters in turn produces chaotic dynamics, and so are not shown here.

Figure 13 shows a selection of phase portraits, projected into the (x, y)-plane, showing the behaviour as b decreases through a succession of periodic and chaotic windows. We chose (a) $b = 45$ (period-9); (b) $b = 40$ (period-7); (c) $b = 35$ (broad-banded chaotic); (d) $b = 30$ (period-5); (e) $b = 28$ (broad-banded chaotic with one fewer loop); (f) $b = 20$ (period-3).

The original 4-D system (14) (Vaidyanathan et al., 2018) also exhibits unbounded growth as $a \to 0$; Figure 14 shows an example of this nonlinear behaviour as a decreases. The lower panel of Figure 14 shows the bifurcation transition sequence as b decreases, terminating on a Hopf Bifurcation at $b \approx 5.4$, in agreement with Eq. (27); when we substitute $(a, c) = (5, 0.5)$ we obtain $b_{4HB} = 5.4167$. Again the results of the linear stability analysis are verified. However, we note the difference in the nonlinear behaviour as b departs from the chaotic regime, in comparison with the 5-D case, shown in Figure 12.

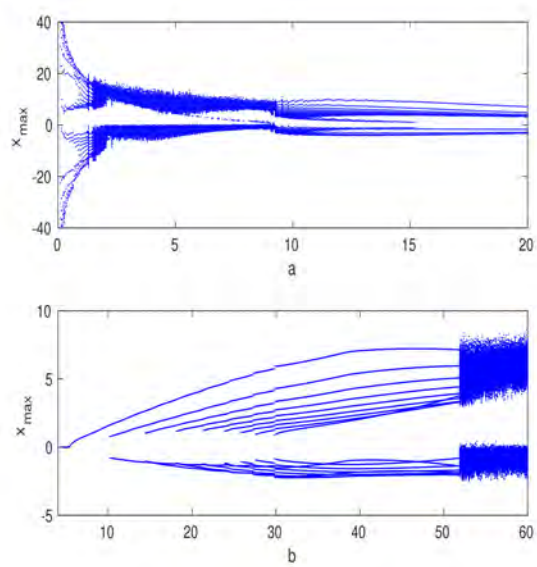

Figure 14: Bifurcation transition plot of x_{max} for the 4-D system (1.2). The upper panel is as a decreases and the lower panel is for b decreasing.

3.6 Dynamics at infinity

3.6.1 5-D weather fluctuation system

The behaviour of x_{max} as a decreases, as shown in Figs 1 and 3, suggests that we consider the dynamics of the 5-D weather fluctuation system (13) as $x \to \infty$ in order to identify the source of the periodic orbit as

$a \to 0$. (Here, x stands for the first state variable y_1 of the 5-D system (13).)

3.6.1.1 Case A

We introduce new variables

$$(y_1, y_2, y_3, y_4, y_5) = (\frac{1}{X}, \frac{Y_2}{X}, \frac{Y_3}{X}, \frac{Y_4}{X}, \frac{Y_5}{X}), t = X\tau. \quad (29)$$

Substitution into (13) gives $\frac{d}{dt} \to \frac{1}{X}\frac{d}{d\tau}$ and

$$\begin{aligned} X_\tau &= (a - bY_2 - Y_4 - pY_5)X^2, \\ Y_{2\tau} &= -Y_2X(-a + bY_2 + Y_4 + pY_5) \\ &\quad +X(1 - Y_2) + Y_3, \\ Y_{3\tau} &= -Y_3X(-a + bY_2 + Y_4 + pY_5) - Y_3X - Y_2, \\ Y_{4\tau} &= -Y_4X(-a + bY_2 + Y_4 + pY_5) - cX(1 + Y_2, \\ Y_{5\tau} &= -Y_5X(-a + bY_2 + Y_4 + pY_5) - dY_2X, \end{aligned} \quad (30)$$

where subscripts denote derivatives with respect to τ.

In order to obtain the dynamics at infinity, we take the limit as $X \to 0$ so that Eq. (30) becomes

$$Y_{2\tau} = Y_3, \quad (31a)$$
$$Y_{3\tau} = -Y_2, \quad (31b)$$
$$Y_{4\tau} = 0, \quad (31c)$$
$$Y_{5\tau} = 0, \quad (31d)$$

together with $X_\tau = 0$. From the equations for $Y_{2\tau} = 0$ and $Y_{3\tau} = 0$, we obtain the fixed point $(Y_2, Y_3) = (0, 0)$; the remaining two equations integrate to give $Y_4 = A_4$ and $Y_5 = A_5$. The stability of this fixed point at infinity is found from the eigenvalues of the four-dimensional Jacobian matrix and we obtain a centre at ∞ with the equation ${Y_2}^2 + {Y_3}^2 = A_1$, where the latter constant is determined from initial conditions. We therefore obtain a system of concentric circles. Moreover we can trivially multiply the equations (31c) and (31d) by Y_4 and Y_5 respectively, combine with the integral of the first two equations to obtain a circle in 4-D space:

$${Y_2}^2 + {Y_3}^2 + {Y_4}^2 + {Y_5}^2 = A. \quad (32)$$

3.6.1.2 Case B

Here, we introduce new variables

$$(y_1, y_2, y_3, y_4, y_5) = (\frac{Y_1}{X}, \frac{1}{X}, \frac{Y_3}{X}, \frac{Y_4}{X}, \frac{Y_5}{X}), t = X\tau. \quad (33)$$

We substitute the new variables into (13) and take the limit as $X \to 0$.

Then we obtain

$$Y_{1\tau} = -{Y_1}^2Y_3, \quad (34a)$$
$$Y_{3\tau} = -Y_1(1 + {Y_3}^2), \quad (34b)$$
$$Y_{4\tau} = -Y_1Y_3Y_4, \quad (34c)$$
$$Y_{5\tau} = -Y_1Y_3Y_5. \quad (34d)$$

If we take the fixed point as $Y_1 = 0$, then the remaining variables are arbitrary. We could also choose $Y_3 = 0$; this gives $Y_1 = 0$, with Y_4 and Y_5 as arbitrary. We could also choose $(Y_4, Y_5) = (0, 0)$ and then either $Y_1 = 0$ with Y_3 arbitrary, or $Y_3 = 0$, giving $Y_1 = 0$.

The equations (34a) and (34b) are independent of Y_4 and Y_5 and can be solved directly to give $Y_3 = Y_1(C_3 - \tau)$, while Y_1 and Y_3 can be eliminated from the remaining two equations to give $Y_4 = C_4Y_5$. We can also solve the equations (34a and (34c) to give $Y_4 = C_1Y_1$. The explicit presence of the τ term in the solution for Y_3 means that the solutions become unbounded as τ increases.

3.6.1.3 Case C

Here, we introduce new variables

$$(y_1, y_2, y_3, y_4, y_5) = (\frac{Y_1}{X}, \frac{Y_2}{X}, \frac{1}{X}, \frac{Y_4}{X}, \frac{Y_5}{X}), t = X\tau. \quad (35)$$

We substitute the new variables into (13) and take the limit as $X \to 0$.

Then we obtain

$$Y_{1\tau} = {Y_1}^2Y_2, \quad (36a)$$
$$Y_{2\tau} = Y_1(1 + {Y_2}^2), \quad (36b)$$
$$Y_{4\tau} = Y_1Y_2(Y_4 - c), \quad (36c)$$
$$Y_{5\tau} = Y_1Y_2Y_5. \quad (36d)$$

Following the approach in the previous subsection, we find that $Y_2 = Y_1(D_1 + \tau)$, $Y_1 = D_2Y_5$ and $Y_4 = D_3Y_5 + c$. Therefore, the solutions to this system grow unbounded as τ increases.

3.7 Case D

Here, we introduce new variables

$$(y_1, y_2, y_3, y_4, y_5) = (\frac{Y_1}{X}, \frac{Y_2}{X}, \frac{Y_3}{X}, \frac{1}{X}, \frac{Y_5}{X}), t = X\tau. \quad (37)$$

We substitute the new variables into (13) and take the limit as $X \to 0$.

Then we obtain

$$Y_{1\tau} = 0, \quad (38a)$$
$$Y_2v_\tau = Y_1Y_3, \quad (38b)$$
$$Y_3w_\tau = -Y_1Y_2. \quad (38c)$$

This has a solution ${Y_2}^2 + {Y_3}^2 = E_1$ and $Y_1 = E_2$, for constants E_1, E_2, whose values depend on initial data. Indeed, we can combine the three equations, by multiplying the first by Y_1 and integrating to give a circle in 3-D phase space at infinity:

$${Y_1}^2 + {Y_2}^2 + {Y_3}^2 = {E_2}^2 + E_1. \quad (39)$$

3.8 The 4-D system

Since Figure 14 shows unbounded growth as $a \to 0$, we summarise the corresponding dynamics at infinity for the 4-D system (14). This was not considered by Vaidyanathan et al. (2018).

3.8.1 Case A

Here, we introduce new variables

$$(y_1, y_2, y_3, y_4) = (\frac{1}{X}, \frac{Y_2}{X}, \frac{Y_3}{X}, \frac{Y_4}{X}), t = X\tau. \tag{40}$$

We substitute the new variables into (14) and take the limit as $X \to 0$.

Then we obtain

$$Y_{2\tau} = Y_3, \tag{41a}$$
$$Y_{3\tau} = -Y_2. \tag{41b}$$

This integrates to give a centre at infinity: ${Y_2}^2 + {Y_3}^2 = A$, where the constant A is determined from initial data.

3.8.1.1 Case B

Here, we introduce new variables

$$(y_1, y_2, y_3, y_4) = (\frac{Y_1}{X}, \frac{1}{X}, \frac{Y_3}{X}, \frac{Y_4}{X}), t = X\tau. \tag{42}$$

We substitute the new variables into (14) and take the limit as $X \to 0$.

Then we obtain

$$Y_{1\tau} = -{Y_1}^2 Y_3, \tag{43a}$$
$$Y_{3\tau} = -Y_1(1 + {Y_3}^2), \tag{43b}$$
$$Y_{4\tau} = -Y_1 Y_3 Y_4. \tag{43c}$$

Following the approach in the previous subsection for the 5-D system (13), we obtain the solution $Y_4 = B_1 Y_1$ and $Y_3 = (B_2 - \tau)Y_1$ for constants B_1, B_2, which are determined from initial data. This solution grows unbounded and is therefore unstable.

3.8.1.2 Case C

Here, we introduce new variables

$$(y_1, y_2, y_3, y_4) = (\frac{Y_1}{X}, \frac{Y_2}{X}, \frac{1}{X}, \frac{Y_4}{X}), t = X\tau. \tag{44}$$

We substitute the new variables into (14) and take the limit as $X \to 0$.

Then we obtain

$$Y_{1\tau} = {Y_1}^2 Y_2, \tag{45a}$$
$$Y_{2\tau} = Y_1(1 + {Y_2}^2), \tag{45b}$$
$$Y_{4\tau} = Y_1 Y_2 Y_4. \tag{45c}$$

This system is identical to that of Case B if we replace Y_3 by Y_2 and change all the signs to be positive. We again therefore find an unbounded and unstable state at infinity, whose solution is given by $Y_4 = C_1 Y_1$ and $Y_2 = Y_1(C_2 + \tau)$, for constants C_j, $j = 1, 2$.

3.8.2 Case D

Here, we introduce new variables

$$(y_1, y_2, y_3, y_4) = (\frac{Y_1}{X}, \frac{Y_2}{X}, \frac{Y_3}{X}, \frac{1}{X}), t = X\tau. \tag{46}$$

We substitute the new variables into (14) and take the limit as $X \to 0$.

Then we obtain

$$Y_{1\tau} = 0, \tag{47a}$$
$$Y_2 v_\tau = Y_1 Y_3, \tag{47b}$$
$$Y_3 w_\tau = -Y_1 Y_2, \tag{47c}$$

with the solution ${Y_1}^2 + {Y_2}^2 + {Y_3}^2 = D$. Again we obtain a centre in the 3-D plane of (Y_1, Y_2, Y_3), with the initial conditions determining the constant of integration.

3.9 Summary of the bifurcation analysis

Although we focused upon the 5-D extension (13) to the 4-D weather fluctuation model (14)) (Vaidyanathan et al., 2018), we found it instructive to compare certain aspects of the behaviours of both models. Both systems can support Hopf bifurcations, but not for the initially prescribed parameter values of $(a, b, c, d, p) = (5, 150, 0.5, 2, 2.5)$ for the 5-D model and $(a, b, c) = (10, 150, 2)$ for the 4-D model. The Hopf bifurcations are most readily seen in the bifurcation transition diagrams for $xmax$ as the parameter b decreases. The values for both models agree with the results of the linear stability theory.

The bifurcation transition diagram for the 5-D system, as b decreases, shows a succession of periodic and chaotic branches (See Figures 12 and 13.) The periodic states decrease through odd periods: we found period-9, period-7, period-5, period-3 and period-1 states, before losing stability in a Hopf bifurcation; each section of periodic states is separated by narrow chaotic branches.

In contrast, once the chaotic behaviour was lost in the 4-D system, only periodic states were observed, with the periodicity reducing systematically as b decreased (see Figure 13 b).

Both 4-D and 5-D weather fluctuation models also exhibit unbounded growth of the trajectories as the parameter a decreases to zero, prompting studies of the dynamics at infinity. For the 5-D system (13), the only parameter which appears in the dynamics at infinity (apart from constants of integration, determined from initial data) is the parameter c. In the 4-D system (14), no parameter appears.

For the 5-D model at infinity, two of the cases yield centres; while the remaining two cases give unbounded

Table 1 The Values of the Circuit Components in the 5-D Circuit (48)

Circuit Component	Value
R_1	$80\,k\Omega$
R_2	$3.2\,k\Omega$
R_3, R_5, R_6, R_8	$400\,k\Omega$
R_7, R_9	$40\,k\Omega$
R_{10}, R_{11}	$800\,k\Omega$
R_{12}	$200\,k\Omega$
$R_{13}, R_{14}, R_{15}, R_{16}$	$100\,k\Omega$
$R_{17}, R_{18}, R_{19}, R_{20}$	$100\,k\Omega$
C_1, C_2, C_3, C_4, C_5	$1\,nF$
The power supplies	± 15 Volts

states. This is similar to the 4-D case. Only the local dynamics depend upon the remaining parameters of the system. Moreover it is the same cases at infinity that admit centres in both the 5-D and 4-D weather fluctuation systems.

4 Circuit Model of the new 5-D hyperchaotic weather fluctuation model with a hyperplane of equilibrium points

In this section, MultiSim (Version 14) is used for the realisation of the proposed system. Figure 15 presents such an analog circuit describing the the new 5-D hyperchaotic weather fluctuation model with a hyperplane of equilibrium points. The designed circuit includes two analog multipliers, 9 operational amplifiers, 20 resistors and 5 capacitors.

By using Kirchhoff's circuit laws, the circuital equations of the designed circuit in Figure 15 are derived as follows:

$$\begin{aligned}
C_1\,\dot{y_1} &= -\tfrac{1}{R_1}y_1 + \tfrac{1}{R_2}y_2 + \tfrac{1}{R_3}y_4 + \tfrac{1}{R_4}y_5\\
C_2\,\dot{y_2} &= \tfrac{1}{R_5}y_1 - \tfrac{1}{R_6}y_2 + \tfrac{1}{10R_7}y_1y_3\\
C_3\,\dot{y_3} &= -\tfrac{1}{R_8}y_3 - \tfrac{1}{10R_9}y_1y_2\\
C_4\,\dot{y_4} &= -\tfrac{1}{R_{10}}y_1 - \tfrac{1}{R_{11}}y_2\\
C_5\,\dot{y_5} &= -\tfrac{1}{R_{12}}y_2
\end{aligned} \tag{48}$$

The values of the circuit components in the 5-D circuit (48) are detailed in Table 1.

Figures 16-19 provide MultiSim simulation results of the 5-D circuit (48). These results obtained using MultiSim are consistent with the results obtained using Matlab simulation and shown in the Figures 5-8.

5 FPGA design of the 5-D hyperchaotic weather fluctuation model

In recent years, the use of FPGAs for the implementation of chaotic systems has increased the attention or researchers. This is due to the flexibility of the devices to create dedicated architectures in a short time and with good performances. The general idea behind the implementation of continuos-time chaotic systems, as the one proposed herein, is to select a way to discretize the system using a numerical method. Among the available methods, one can find one-step and multi-step methods, and even special methods as the one given in (Zaqueros-Martinez et al., 2022). However, it has been demonstrated that one-step methods require the lowest hardware resources, as shown in (Vaidyanathan et al., 2021). One of the most popular because of its simplicity of hardware implementation and low resource usage is the well-known Forward Euler. Other used methods that one can find in the literature are the Backward Euler, fourth order Runge-Kutta, trapezoidal method, among many others. The important thing to note is that depending on whether the methods are explicit or implicit, one-step or multi-step, the complexity will change drastically as well as the use of resources and directly influencing the speed of the system. On the one hand, researchers have noted that using an implicit method requires a larger number of operations to obtain x_{n+1}. On the other hand, explicit methods are a good option for fast prototyping using FPGAs, and they are applied herein.

Once a numerical method has been selected, the designer must ensure that the system works correctly using a limited amount of bits to reach a good resolution, i.e., one must ensure that the number of bits available for the design is sufficient to reproduce the chaotic behavior. Fixed-point computer arithmetic is used when working with this type of architecture, therefore it is necessary to perform a fixed point analysis before starting with the hardware description to correctly select the amount of bits to represent the integer and fractional part of the magnitudes of the state variables of the chaotic system. In this manner, this work shows the application of the Forward Euler and trapezoidal methods to implement the new chaotic system that generated hyperchaotic behavior.

The Forward Euler method is based on the iterative equation shown in (49), and when applied to the new 5-D system, the discretized equations are given in 50. From the discretized system, one can see that they require the use of multipliers, adders and subtractors for the FPGA implementation.

$$x_{n+1} = x_n + hf(x_n, t_n) \tag{49}$$

$$\begin{aligned}
y_{1_{n+1}} &= y_{1_n} + h[-ay_{1_n} + by_{2_n} + y_{4_n} + py_{5_n}]\\
y_{2_{n+1}} &= y_{2_n} + h[y_{1_n} - y_{2_n} + y_{1_n}y_{3_n}]\\
y_{3_{n+1}} &= y_{3_n} + h[-y_{3_n} - y_{1_n}y_{2_n}]\\
y_{4_{n+1}} &= y_{4_n} + h[-c(y_{1_n} + y_{2_n})]\\
y_{5_{n+1}} &= y_{5_n} + h[-dy_{2_n}]
\end{aligned} \tag{50}$$

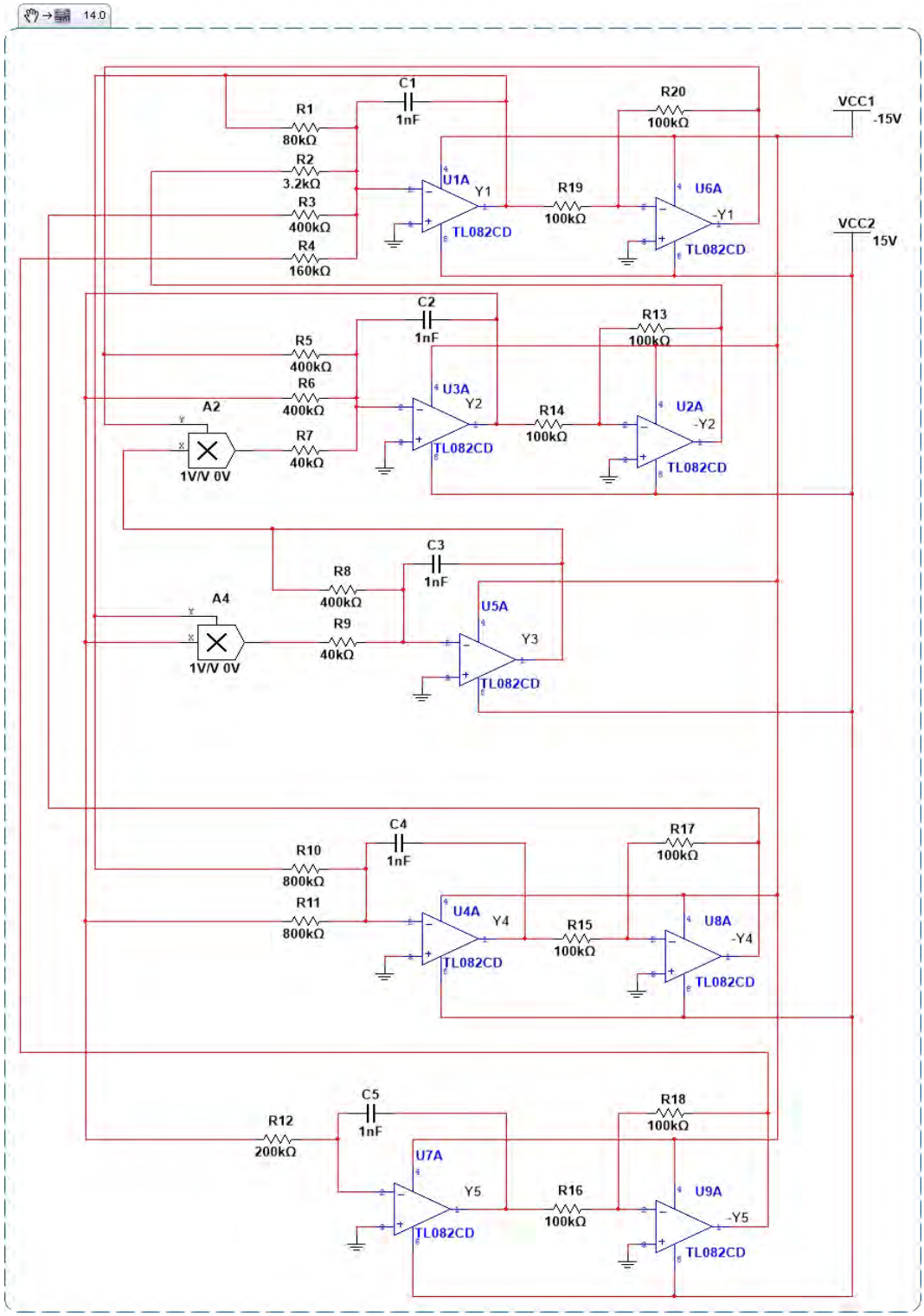

Figure 15: Circuit Design of the new 5-D hyperchaotic weather fluctuation model (48) with a line of equilibrium points

.

To implement the system with the trapezoidal method, the same process as in the previous case is carried out, but using the equation shown in (51), the resulting discretized system is shown in (52).

$$x_{n+1} = x_n + \frac{h}{2}\left[f(x_n, t_n) + f(x_{n+1}, t_{n+1})\right] \tag{51}$$

As one sees, this Trapezoidal algorithm is implicit, that is x_{n+1} is a function of itself, so it is necessary to calculate the x_{n+1} term on the right hand side of the

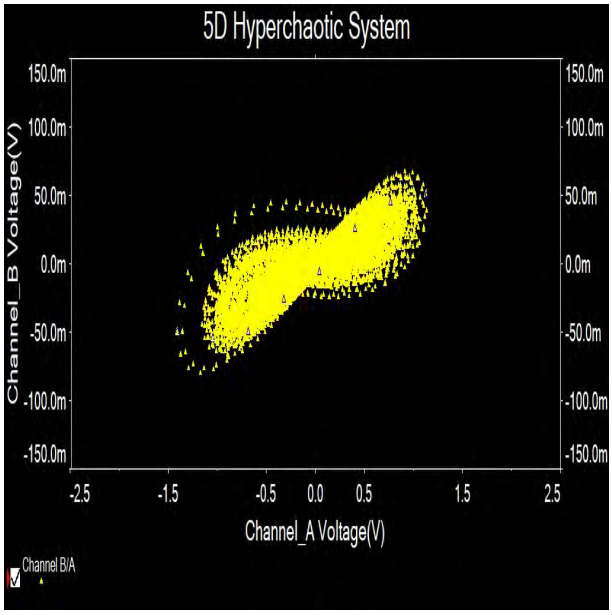

Figure 16: Signal plot simulated in MultiSim for the 5-D hyperchaotic weather fluctuation hyperchaotic system (48) in (y_1, y_2) plane

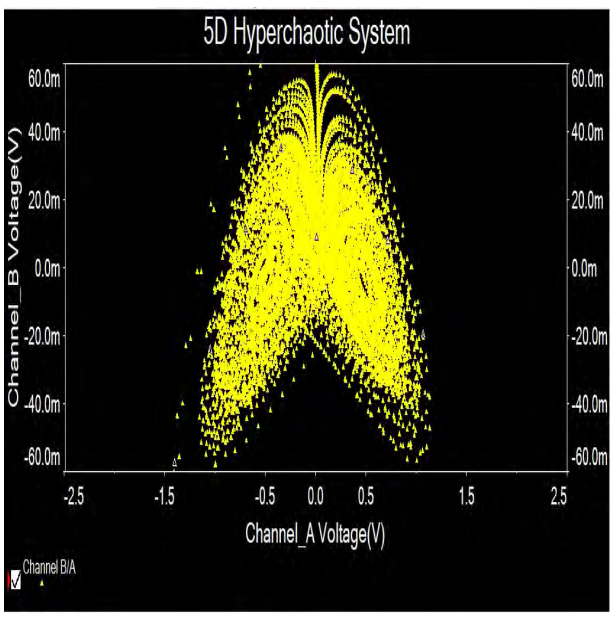

Figure 17: Signal plot simulated in MultiSim for the 5-D hyperchaotic weather fluctuation hyperchaotic system (48) in (y_1, y_3) plane

equation with some other method, which increases the computational cost.

$$
\begin{aligned}
y_{1_{n+1}} &= y_{1_n} + \tfrac{h}{2}[(-ay_{1_n} + by_{2_n} + y_{4_n} + py_{5_n}) \\
&\quad +(-ay_{1_{n+1}} + by_{2_{n+1}} + y_{4_{n+1}} + py_{5_{n+1}})]] \\
y_{2_{n+1}} &= y_{2_n} + \tfrac{h}{2}[(y_{1_n} - y_{2_n} + y_{1_n}y_{3_n}) \\
&\quad +(y_{1_{n+1}} - y_{2_{n+1}} + y_{1_{n+1}}y_{3_{n+1}})]] \\
y_{3_{n+1}} &= y_{3_n} + \tfrac{h}{2}[-y_{3_n} - y_{1_n}y_{2_n} \\
&\quad -y_{3_{n+1}} - y_{1_{n+1}}y_{2_{n+1}}] \\
y_{4_{n+1}} &= y_{4_n} + \tfrac{h}{2}[-c(y_{1_n} + y_{2_n}) - c(y_{1_{n+1}} + y_{2_{n+1}})] \\
y_{5_{n+1}} &= y_{5_n} + \tfrac{h}{2}[-dy_{2_n} - dy_{2_{n+1}}]
\end{aligned}
\tag{52}
$$

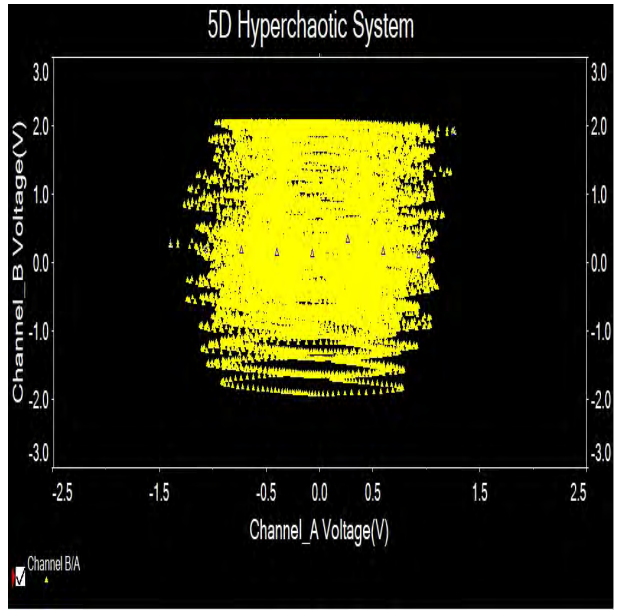

Figure 18: Signal plot simulated in MultiSim for the 5-D hyperchaotic weather fluctuation hyperchaotic system (48) in (y_1, y_4) plane

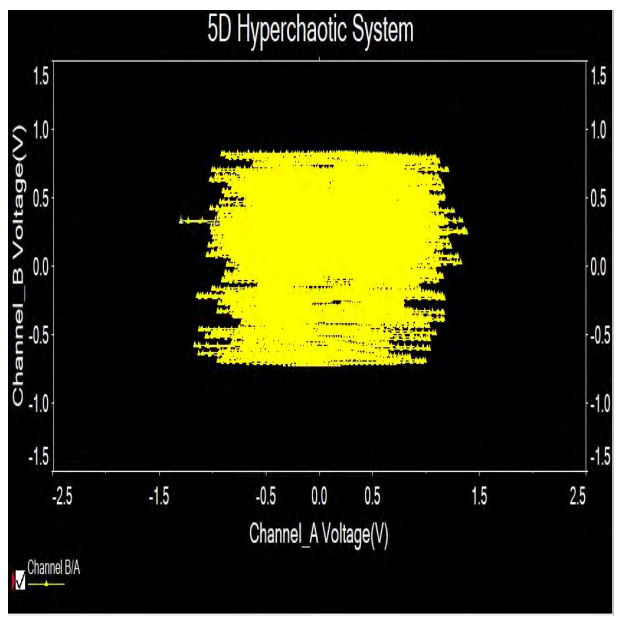

Figure 19: Signal plot simulated in MultiSim for the 5-D hyperchaotic weather fluctuation hyperchaotic system (48) in (y_1, y_5) plane

After performing an analysis of the discretized system and using a 64-bit architecture, a fixed-point format of 9.55 was chosen, one bit for the sign, 8 for the integer part, and 55 for the fractional part. It is worth mentioning that this 9.55 format is set by computer arithmetic and does not depend significantly on the amplitudes of the state variables. For example, simulation results for this 5-D system taking into account all state variables provide the range $[-68.2236, 21.3886]$, but in the discretization, an analysis of all the internal

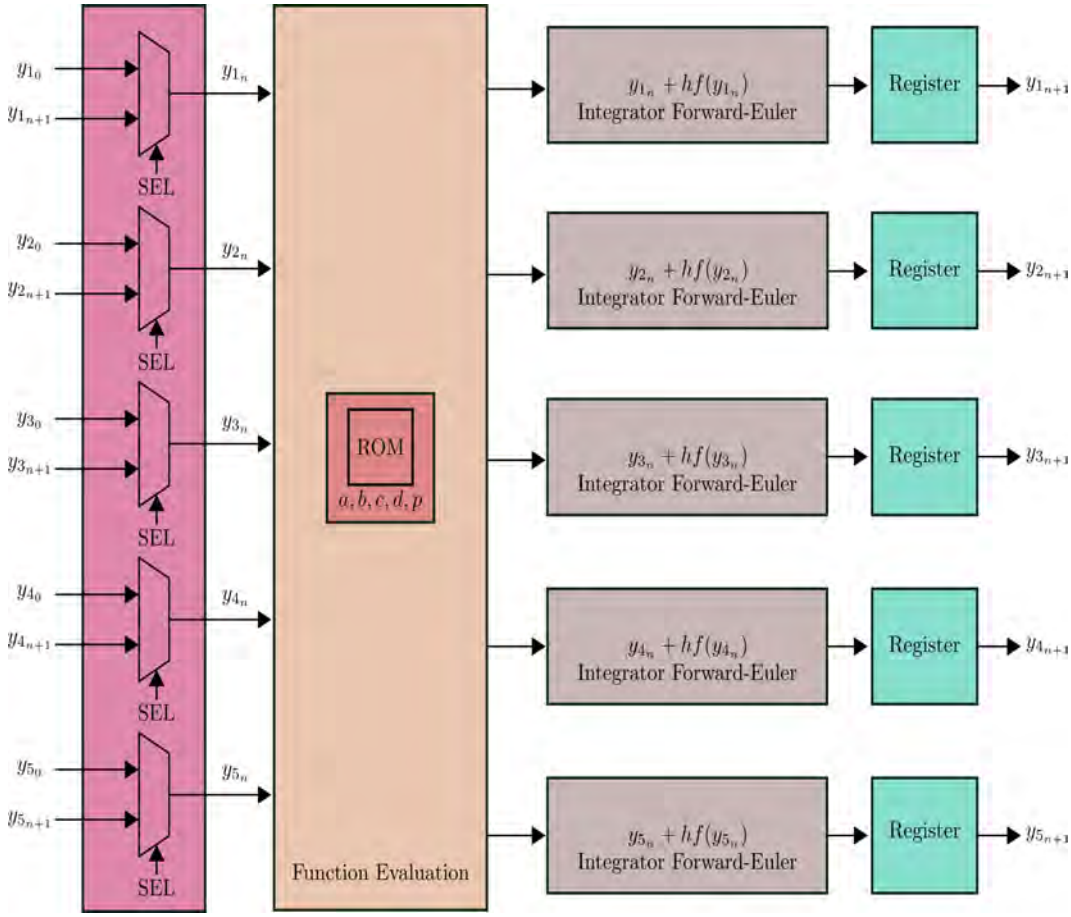

Figure 20: Block diagram of the new 5-D system given in discretized form with the Forward Euler method.

Table 2 Hardware resources for the implementation of the 5-D system by using the FPGA Basys 3 Xilinx Artix-7 XC7A35T-ICPG236C, and by applying the Forward Euler and Trapezoidal methods with $h = 0.001$.

Resources	Forward Euler	Trapezoidal	Available
LUTs	10392	15792	20,800
FF	962	1823	41,600
DSP	39	82	90
Multipliers	12	29	–
Adders	7	24	–
Subtractors	5	10	–
Clock cycles by Iteration	2	3	-
Latency(ns)	80	120	-

arithmetic operations resulted in an absolute range of $[-119.9722, 144.9970]$.

Figure 20 shows the block diagram of the implementation of the system using Forward Euler method, multiplexers are used to be able to load the initial condition of the system and subsequently feed back the output, a read only memory (ROM) is used to store all the constants used in the additions and multiplications of the discretized equations. The hardware resources used for each numerical method are listed in Table 2. Finally, the experimental hyperchaotic attractors are shown in Figures 21-24. These results confirm the usefulness of using FPGAs in the fast prototyping of hyperchaotic systems. The experimental setup showing the oscilloscope is shown in Figure 25.

6 Conclusions

High-dimensional hyperchaotic systems have several engineering applications such as secure communications, steganography, cryptosystems, pseudo-random number generators, etc. We reported new results of a 5-D hyperchaotic weather fluctuation model, which was designed mathematically by means of introducing two state feedback controllers in the 3-D Vallis weather fluctuation model (1986). We showed that the new hyperchaotic system has a line of equilibrium points and deduced that the 5-D hyperchaotic weather fluctuation model has hidden attractors. We performed a detailed bifurcation analysis with standard tools such as

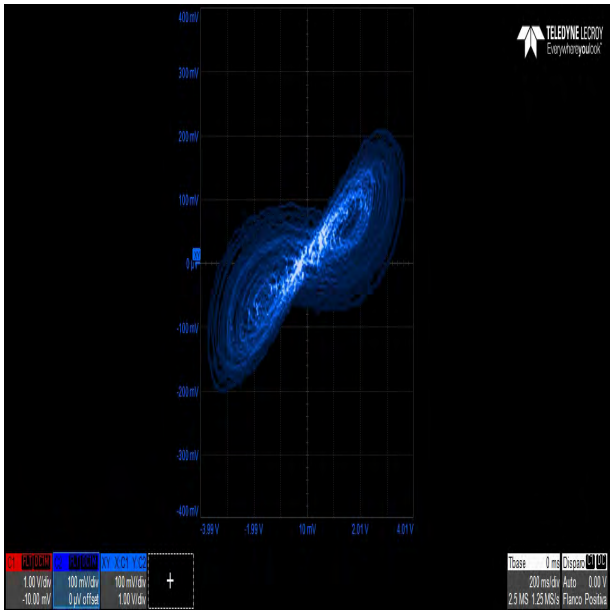

Figure 21: Attractor of the 5-D hyperchaotic weather fluctuation system from the FPGA implementation by applying the Forward Euler method with step-size $h = 0.001$ in (y_1, y_2) plane

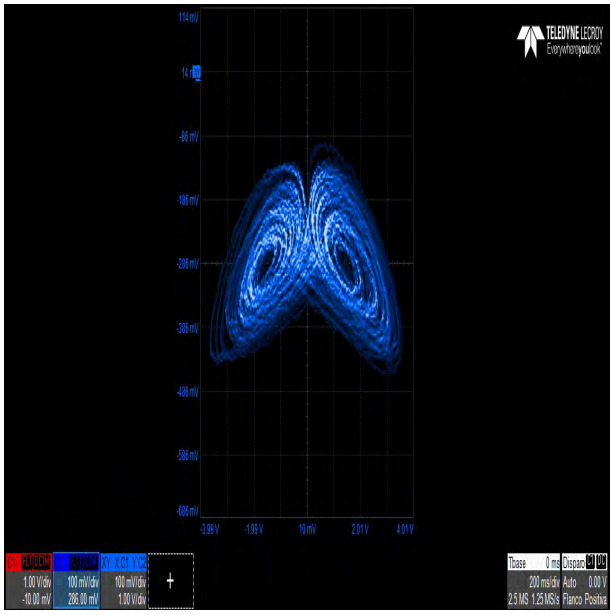

Figure 22: Attractor of the 5-D hyperchaotic weather fluctuation system from the FPGA implementation by applying the Forward Euler method with step-size $h = 0.001$ in (y_1, y_3) plane

bifurcation diagrams and Lyapunov exponents to study the intrinsic properties of the 5-D weather fluctuation model with respect to changes in the system constants. Next, we designed an electronic circuit of the 5-D weather fluctuation model using MultiSim (Version 14). The new 5-D hyperchaotic weather fluctuation model was implemented in FPGA by applying two one-step numerical methods, *viz.* Forward Euler and Trapezoidal

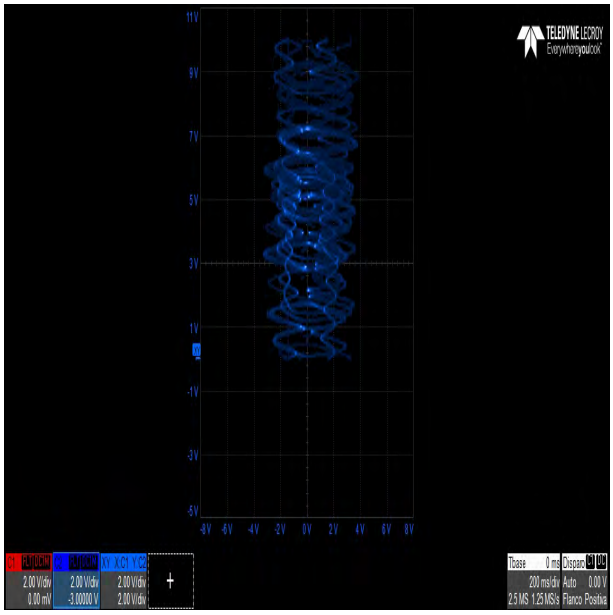

Figure 23: Attractor of the 5-D hyperchaotic weather fluctuation system from the FPGA implementation by applying the Forward Euler method with step-size $h = 0.001$ in (y_1, y_4) plane

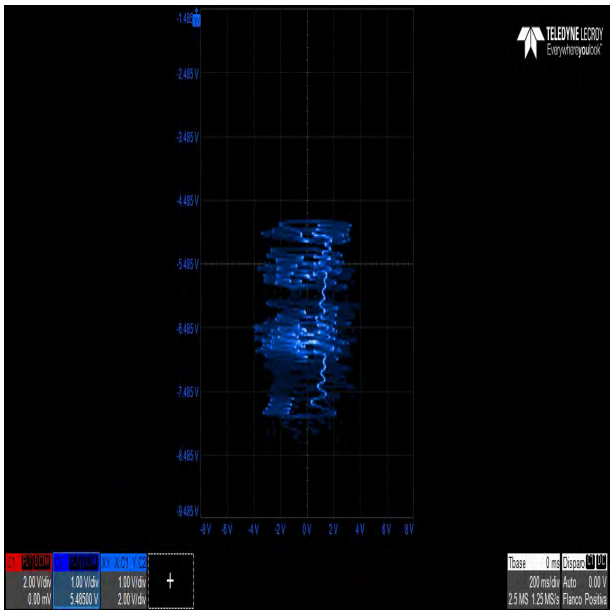

Figure 24: Attractor of the 5-D hyperchaotic weather fluctuation system from the FPGA implementation by applying the Forward Euler method with step-size $h = 0.001$ in (y_1, y_5) plane

rule. Experimental attractors for the 5-D hyperchaotic model were shown from an oscilloscope. Hardware resources used for our FPGA design were displayed in a table.

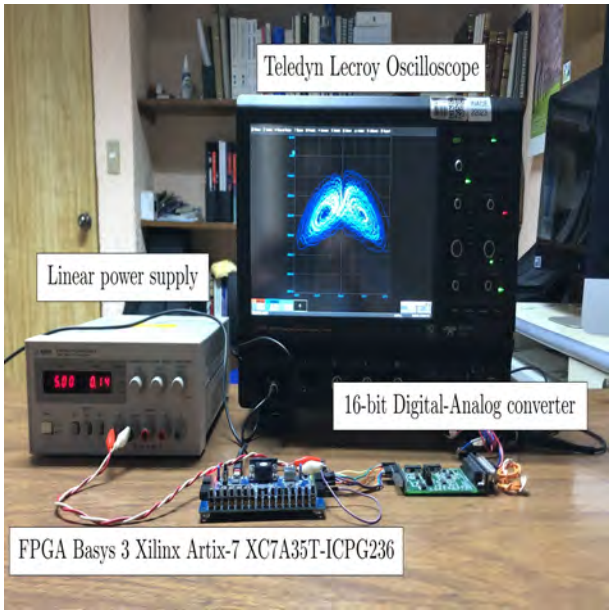

Figure 25: Experimental setup to implement the 5-D system using a FPGA Basys 3 Xilinx Artix-7 XC7A35T-ICPG236, a 16-bit Digital-Analog converter, a linear power supply and a Teledyne Lecroy oscilloscope to visualize the attractor.

References

Almasoud, A. S. (2023). Intelligent deep learning enabled wild forest fire detection system. *Computer Systems Science and Engineering*, 44(2):1485 – 1498.

Bae, H. J. and Koumoutsakos, P. (2022). Scientific multi-agent reinforcement learning for wall-models of turbulent flows. *Nature Communications*, 13(1). Article ID 1443.

Bhardwaj, K. and Srivastava, M. (2022). Mathematical framework for three cross-over memristor and its realization employing OTAs. *Circuit World*, 48(2):160 – 173.

Bhat, J. and Moon, A. H. (2022). Color image encryption and authentication using dynamic DNA encoding and hyper chaotic System. *Expert Systems with Applications*, 206. Article ID 117861.

Cai, J. and He, J. (2022). A new hyperchaotic system generated by an external periodic excitation and its image encryption application. *Journal of Advanced Computational Intelligence and Intelligent Informatics*, 26(3):418 – 430.

Carbajal-Gomez, V. H., Tlelo-Cuautle, E., Muñoz-Pacheco, J. M., de la Fraga, L. G., Sanchez-Lopez, C., and Fernandez-Fernandez, F. V. (2019). Optimization and CMOS design of chaotic oscillators robust to PVT variations. *Integration*, 65:32–42.

Chen, Z.-M. (1993). A note on Kaplan-Yorke-type estimates on the fractal dimension of chaotic attractors. *Chaos, Solitons & Fractals*, 3(5):575–582.

Dachraoui, C., Mouelhi, A., Drissi, C., and Labidi, S. (2022). Hybrid fuzzy level set approach for multiple sclerosis lesions assessment in magnetic resonance brain images. *International Journal of Modelling, Identification and Control*, 40(3):260 – 270.

Dong, C. and Wang, J. (2022). Hidden and coexisting attractors in a novel 4d hyperchaotic system with no equilibrium point. *Fractal and Fractional*, 6(6). Article ID 306.

Doungmo Goufo, E. F. (2022). Linear and rotational fractal design for multiwing hyperchaotic systems with triangle and square shapes. *Chaos, Solitons and Fractals*, 161. Article ID 112283.

Frederickson, P., Kaplan, J. L., Yorke, E. D., and Yorke, J. A. (1983). The Liapunov dimension of strange attractors. *Journal of Differential Equations*, 49(2):185–207.

Fu, H. and Lei, T. (2022). Adomian decomposition, dynamic analysis and circuit Implementation of a 5D fractional-order hyperchaotic system. *Symmetry*, 14(3). Article ID 484.

Fujita, S. and Tanaka, T. (2022). Two current systems in the preliminary phase of sudden commencements in the magnetosphere. *Earth, Planets and Space*, 74(1). Article ID 66.

Gaouzi, K., Fadil, H. E., El-Idrissi, Z., and Lassioui, A. (2022). Digital implementation of model predictive control of an inverter for electric vehicles applications. *International Journal of Modelling, Identification and Control*, 40(3):210 – 218.

Hassani, H., Mansouri, A., and Ahaitouf, A. (2022). Robust hybrid controller for quadrotor uav under disturbances. *International Journal of Modelling, Identification and Control*, 40(3):195 – 203.

Liu, X. and Wang, J. (2022). The simplest memristor circuit with hyperchaos. *Frontiers in Physics*, 10. Article ID 904200.

Lopez-Rodriguez, V. and Ceballos, H. G. (2022). Modeling scientometric indicators using a statistical data ontology. *Journal of Big Data*, 9(1). Article ID 9.

Meng, Y. and Shao, C. (2022). Physics-informed ensemble learning for online joint strength prediction in ultrasonic metal welding. *Mechanical Systems and Signal Processing*, 181. Article ID 109473.

Nichols, J. M., Todd, M. D., Seaver, M., Trickey, S. T., Pecora, L. M., and Moniz, L. (2003). Controlling system dimension: A class of real systems that obey

the kaplan-yorke conjecture. *Proceedings of the National Academy of Sciences*, 100(26):15299–15303.

Okasha, M., Kralev, J. K., and Islam, M. (2022). Investigation and realisation of pid and lqr control methods in parrot mambo minidrone. *International Journal of Modelling, Identification and Control*, 40(3):249 – 259.

Peng, X., Zeng, Y., and Xie, Q. (2021). Dynamics analysis of a 5-dimensional hyperchaotic system with conservative flows under perturbation. *Chinese Physics B*, 30(10). Article ID 100502.

Petrzela, J. (2022). Chaotic and hyperchaotic dynamics of a Clapp oscillator. *Mathematics*, 10(11). Article ID 1868.

Petrzela, J. and Rujzl, M. (2022). Chaotic oscillations in cascoded and darlington-type amplifier having generalized transistors. *Mathematics*, 10(3). Article ID 532.

Qian, X., Luo, Y., and Zhang, P. (2022). Research on the emerging mechanism of complex networks community dividing based on cellular automata. *International Journal of Modelling, Identification and Control*, 40(3):239 – 248.

Ratier, A. and Charles, S. (2022). Accumulation-depuration data collection in support of toxicokinetic modelling. *Scientific Data*, 9(1). Article ID 130.

Silva-Juarez, A., Tlelo-Cuautle, E., and de la Fraga, L. G. (2022). FPAA-based implementation of fractional-order multidirectional multiscroll chaotic oscillators. In *Fractional Order Systems*, pages 341–374. Elsevier.

Tanaka, G. and Nakane, R. (2022). Simulation platform for pattern recognition based on reservoir computing with memristor networks. *Scientific Reports*, 12(1). Article ID 9868.

Tang, X. and Liu, Z. (2022). Robust adaptive smc for uncertain singular delayed systems via observer. *International Journal of Modelling, Identification and Control*, 40(2):105 – 113.

Thomas, F. and Mija, S. (2022). Hover autopilot design for an un-crewed helicopter using static output feedback controller. *International Journal of Modelling, Identification and Control*, 40(2):137 – 150.

Tiglio, M. and Villanueva, A. (2022). Reduced order and surrogate models for gravitational waves. *Living Reviews in Relativity*, 25(1). Article ID 2.

Vaidyanathan, S., Azar, A. T., Rajagopal, K., Sambas, A., Kacar, S., and Cavusoglu, U. (2018). A new hyperchaotic temperature fluctuations model, its circuit simulation, fpga implementation and an application to image encryption. *International Journal of Simulation and Process Modelling*, 13(3):281 – 296.

Vaidyanathan, S., Sambas, A., Tlelo-Cuautle, E., Abd El-Latif, A. A., Abd-El-Atty, B., Guillén-Fernández, O., Benkouider, K., Mohamed, M. A., Mamat, M., and Ibrahim, M. A. H. (2021). A new 4-D multi-stable hyperchaotic system with no balance point: Bifurcation analysis, circuit simulation, FPGA realization and image cryptosystem. *IEEE Access*, 9:144555–144573.

Vallis, G. K. (1986). El nino: A chaotic dynamical system? *Science*, 231:1289.

Wu, H., Wang, C., Zhou, Y., Xie, W., and Chen, C. (2022). A study on photovoltaic charging strategy of electric vehicles with multi-objective constraints. *International Journal of Modelling, Identification and Control*, 40(3):231 – 238.

Yoon, J.-Y. and Kim, B. (2022). Examination of sub-harmonic responses along with various initial conditions induced by multi-staged clutch damper system. *Scientific Reports*, 12(1). Article ID 11339.

Zahorán, L. and Kovács, A. (2022). ProSeqqo: A generic solver for process planning and sequencing in industrial robotics. *Robotics and Computer-Integrated Manufacturing*, 78. Article ID 102387.

Zaqueros-Martinez, J., Rodriguez-Gomez, G., Tlelo-Cuautle, E., and Orihuela-Espina, F. (2022). Trigonometric polynomials methods to simulate oscillating chaotic systems. In *AIP Conference Proceedings*, volume 2425, page 420035. AIP Publishing LLC.

Zhang, Z. and Huang, L. (2022). A new 5d hamiltonian conservative hyperchaotic system with four center type equilibrium points, wide range and coexisting hyperchaotic orbits. *Nonlinear Dynamics*, 108(1):637 – 652.